Pneumatic Non-Equibiaxial Cell Stretching Device With Live-Cell Imaging

Jue Wang, *Graduate Student Member, IEEE*, Aritra Chatterjee, Clarisse Zigan, Maya Alborn, Deva D. Chan, and Alex Chortos, *Member, IEEE*

Abstract*—*Objective: **Adherent cell behavior is influenced by a complex interplay of factors, including chemical and mechanical signals. In vitro experiments that mimic the mechanical environment experienced by cells in vivo are crucial for understanding cellular behavior and the progression of disease. In this study, we developed and validated a low-cost pneumatically-controlled cell stretcher with independent control of strain in two directions of a membrane, enabling unequal biaxial stretching and real-time microscopy during actuation.** ***Methods:*** **The stretching was achieved by two independent pneumatic channels controlled by electrical signals. We used finite element simulations to compute the membrane's strain field and particle tracking algorithms based on image processing techniques to validate the strain fields and measure the cell orientation and morphology.** ***Results:*** **The device can supply uniaxial, equibiaxial, and unequal biaxial stretching up to 15% strain in each direction at a frequency of 1 Hz, with a strain measurement error of less than 1%. Through live cell imaging, we determined that distinct stretching patterns elicited differing responses and alterations in cell orientation and morphology, particularly in terms of cell length and area.** ***Conclusion:*** **The device successfully provides a large, uniform, and variable strain field for cell experiments, while also enabling real-time, live cell imaging.** ***Significance:*** **This scalable, low-cost platform provides mechanical stimulation to cell cultures by independently controlling strains in two directions. This could contribute to a deeper understanding of cellular response to bio-realistic strains and could be useful for future in vitro drug testing platforms.**

***Index Terms*—Mechanobiology, Cell stretching devices, Live-cell images, Finite element simulation, Cell orientation and morphology.**

Manuscript received 18 June 2023; revised 20 August 2023; accepted 20 September 2023. Date of publication 25 September 2023; date of current version 26 February 2024. The work of Jue Wang and Alex Chortos was supported by the startup package of the Mechanical Engineering Department at Purdue. The work of Aritra Chatterjee, Maya Alborn, and Clarisse Zigan was supported by NSF under Grant 2149946. The work of Aritra Chatterjee and Deva D. Chan was supported by NSF under Grant BII 2120200. *(Corresponding author: Alex Chortos.)*

Jue Wang is with the School of Mechanical Engineering, Purdue University, USA.

Aritra Chatterjee, Clarisse Zigan, Maya Alborn, and Deva D. Chan are with the Weldon School of Biomedical Engineering, Purdue University, USA.

Alex Chortos is with the School of Mechanical Engineering, Purdue University, West Lafayette, IN 47906 USA (e-mail: achortos@purdue.edu).

This article has supplementary downloadable material available at https://doi.org/10.1109/TBME.2023.3319013, provided by the authors.

Digital Object Identifier 10.1109/TBME.2023.3319013

I. Introduction

ADHERENT Cell behavior is governed by an interplay of internal and external factors that include chemical and mechanical signals. These stimuli modulate cellular processes such as metabolism and extracellular matrix remodeling. In tissues such as lungs, arteries, cartilage and the musculoskeletal system, mechanical stimuli play an important role in regulating structure and function [1]. The biological response is highly dependent on the parameters of the mechanical stimulation (e.g., uniaxial vs biaxial, strain magnitude, frequency). The ability to mimic the complex mechanical stimuli is crucial to understanding mechanobiology in healthy tissues and diseases such as cardiac fibrosis [2], [3], [4], [5], idiopathic pulmonary fibrosis [6], [7], as well as musculoskeletal disorders [8] and connective tissue diseases [9].

Many cell stretching devices employ electrical actuators such as stepper motors [10], [11], [12], DC motors [13], voice coil motors [14], dielectric elastomer actuators (DEAs) [15] and shape memory alloys [16]. Commercial entities like Strex Inc. and CellScale also utilize motor-controlled actuation in their products. These electromechanical systems can have high precision and can include feedback. However, they are typically costly, limiting their use in large scale experiments. Furthermore, electrothermal heat generation can significantly affect temperature-sensitive cell culture experiments. Pneumatic actuators [17], [18], [19], [20] have lower construction and maintenance costs and smoother motion due to continuous air flow. In addition, pneumatic systems pose a reduced risk of temperature fluctuations in sensitive incubator environments and a lower risk of contamination since the mechanical components do not come into direct contact with the cell culture apparatus. Some pneumatic systems [17], [21], including commercial products from FlexCell, require lubricants at the bottom of the membrane. These lubricants may interact with or seep into stretching membranes, affecting the behavior of cells. [22]

Regarding the functionality of cell stretching devices, uniaxial [11], [22], equibiaxial, and equiaxial [23], [24], [25], [26] stretching methods are predominantly employed due to their relatively simple actuator designs. However, some tissues experience anisotropic mechanical cues. For example, some regions of the heart experience nearly uniaxial strains, some experience nearly equiaxial strains, while most exhibit non-equibiaxial strains. [27] Consequently, non-equibiaxial cell stretching devices provide a platform to facilitate a deeper understanding of cellular behavior relevant to these tissues and disease states. [28]

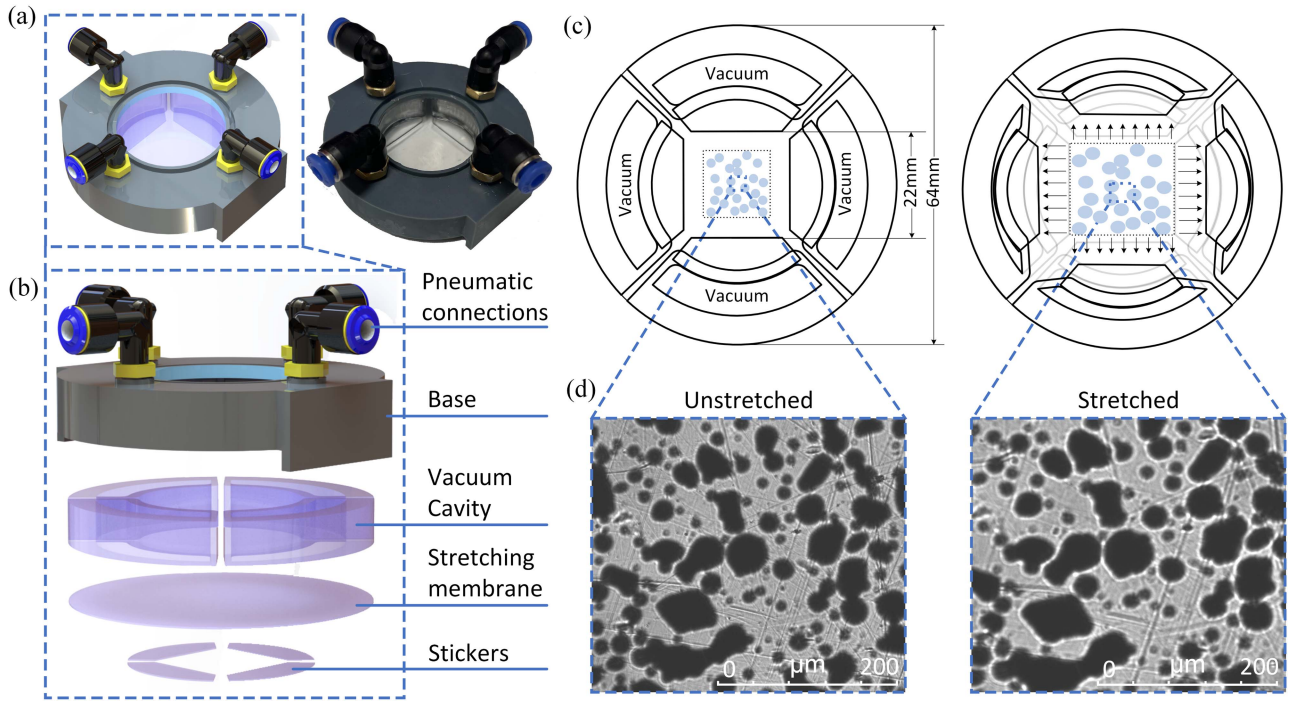

Fig. 1. Design and principle of biaxial cell stretcher. (a) The 3D model and actual device of biaxial cell stretcher. (b) The explosion diagram of biaxial cell stretcher. (c) The dimension and principle of biaxial cell stretcher. (d) Stretching of a speckle pattern.

Currently, few studies focus on non-equibiaxial stretching. Wong et al. [28] and Hu et al. [29] proposed motor-driven non-equibiaxial stretching devices, but these systems preclude live-cell imaging. Tremblay et al. [30] introduced a pneumatic cell stretching device with two independent channels but did not demonstrate non-equibiaxial stretching; the small deformation chamber also hindered the generation of a uniform strain area.

Essential design features for a versatile stretching device that can be applied to various cell study systems include independent control of amplitude and frequency in two orthogonal directions, maintenance of strain homogeneity in thin planar materials, and compatibility with high-resolution optical imaging for real-time data acquisition. To address the limitations of currently available designs, in this work, we have developed and validated a pneumatically controlled cell stretcher with independent control of strain in two directions of a microscopy-compatible membrane. In-plane actuation allows large area uniform non-equibiaxial stretching and real-time microscopy during actuation. Our device is sized similarly to 60-mm petri dishes, making it compact and lightweight. Furthermore, the pneumatic control system can accommodate control of multiple parallel devices under identical actuation conditions.

II. Materials & Methods

A. Design and Fabrication of Biaxial Cell Stretcher

The design of the biaxial cell stretcher is depicted in Fig. 1(a). It consists of 4 main parts: stretcher base, vacuum cavity, stretching membrane, and stickers. The design of the base enables mounting onto an inverted microscope stage for live-cell imaging and connections with the pneumatic system. Four quarter-circular vacuum cavities generate a biaxial stretch, with two opposing cavities connected to a single pneumatic channel to ensure uniform strain in each direction. Vacuum pressure generates shrinkage of cavities' inner shell, stretching the membrane attached to the shell's bottom. Rigid stickers at the edges of the membrane guide the deformation of the membrane to enable uniform strains. The working area is defined by the size of stickers, which is a 22 mm × 22 mm square as shown in Fig. 1(b). We used spray paint to create a speckle pattern to track strain under the microscope. Fig. 1(c) and (d) depicts the deformation on the membrane when we applied non-equibiaxial stretching, which demonstrates the basic functionality of the stretcher in this article.

The base is made by stereolithography (SLA) 3D printing using a Phrozen 8 k printer with 8 k Aqua Gray resin and cured in an oven at 70 °C for 24 hours to ensure biocompatibility. [31] Both cavities and membrane are made of polydimethylsiloxane (PDMS) Sylgard 184 (Dow Corning, USA) with base to cross-linker ratio 17.5:1 and fabricated using molds which are printed with the same printer. The mold has two parts: the middle part defines the vacuum cavity while the outer part of the mold defines the outer shell of the cavities. The Sylgard 184 was mixed using a centrifugal mixer for 4 min and was subsequently centrifuged for 30 s to remove the bubbles. After pouring the Sylgard 184 into the mold, the Sylgard 184 was degassed for 30 min in a vacuum chamber. Following this, the molds with uncured PDMS 184 are put into the oven at 60 °C for 24 hours. The membranes are fabricated by blade coating uncured Sylgard 184 to a uniform thickness of 0.4 mm onto glass coated with non-stick Bytac coating (Cole-Parmer Bytac D1069324 Surface Protector, Fisher). Following this, the membrane was cured in an oven at 60 °C

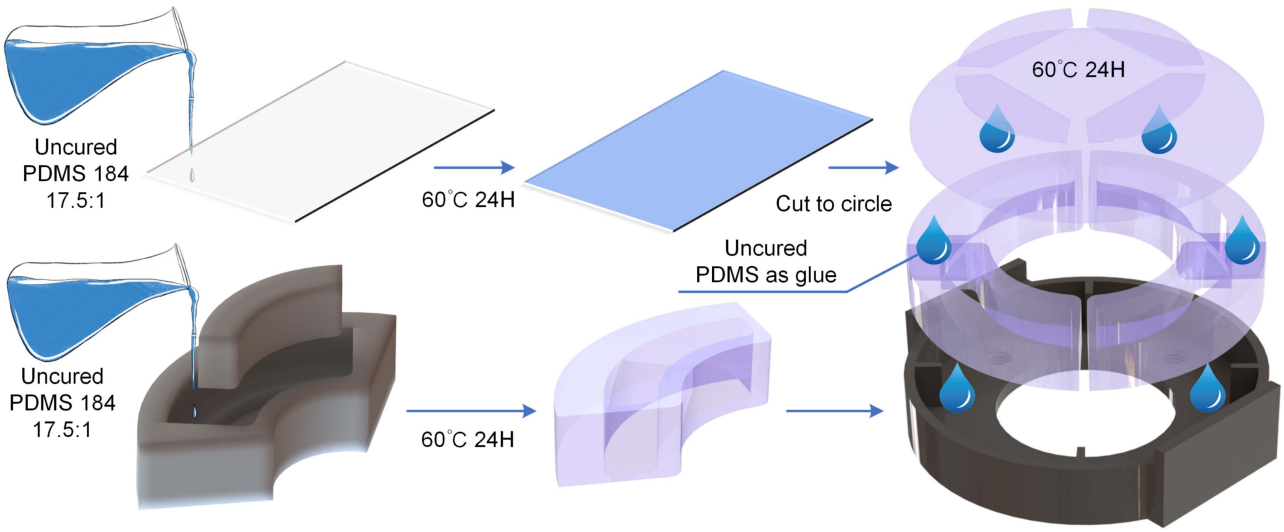

Fig. 2. Fabrication process of biaxial cell-stretcher.

for 24 hours. The rigid stickers laser cut from a $1/32''$-thick acrylic sheet. The inner and outer diameter of the quarter-circular cavities are 34 mm and 64 mm, respectively. The thickness of the stretching membrane attached to the cavities is 0.4 mm.

To ensure the whole device is biocompatible, uncured Sylgard 184 was used to adhere the individual components (base, vacuum cavities, stretching membrane and stickers) together. The entire device was placed in an oven at 60 °C for 24 hours to cure the Sylgard 184 adhesive. (Fig. 2)

All materials in contact with culture media were tested separately for biocompatibility. We also tested for biocompatibility of the entire system by performing live-dead staining on 3T3 fibroblasts cultured using DMEM +10% FBS+1% Pen Strep inside the cell stretcher system for 24 hours under standard culture conditions (37 °C, 95% humidity, 5% CO_2)

B. Dual-Channel Pneumatic Control System

Negative pressure was modulated using a vacuum generator (Festo VAD 1/4) that was driven by positive pressure from 0 to $100PSI$ and controlled using a Alicat Electro-pneumatic Transducer (PCD-series). $0-5\,\mathrm{V}$ analog control signals for the Alicat were generated using digital-to-analog converters (MPC4725) controlled using an Arduino (Mega 2560). The communication between the Arduino and MPC4725 used an I2C interface. However, controlling the two actuation directions independently requires two channel inputs while the Arduino has only one hardware I2C channel. We used software I2C to simulate two channels to communicate with two MPC4725 converters. (Fig. 3)

C. Mechanical Characterization of PDMS Used in the Cell Stretcher

We examined the material properties of Sylgard 184 with a 17.5:1 ratio by conducting uniaxial tensile tests. Dog-bone samples were mounted onto an Electroforce 5500 system. The samples were loaded at $10\,\mathrm{mm/min}$ until failure. In total, five samples were tested. The Young's modulus extracted from the linear strain region (10%) was found to be 303.3 ± 11.6 kPa. In addition, the elongation at break for the samples was 238.9%. (Fig. S1)

D. Finite Element (FE) Simulation of Cell Stretcher

To predict the strain fields on the membrane under different vacuum inputs, finite element (FE) simulations were performed using COMSOL (COMSOL, Inc., USA). The 3D model was made by Solidworks and imported into COMSOL for analysis using the Solid Mechanics module. PDMS was modeled as a linear elastic material with Young's Modulus of $303\,\mathrm{kPa}$ as derived above and Poisson's ratio of 0.43. The base made of SLA resin was assigned a Young's Modulus of $2.2\,\mathrm{GPa}$ and Poisson's ratio of 0.4. The acrylic stickers were assigned a Young's Modulus of $2.5\,\mathrm{GPa}$ and Poisson's ratio of 0.4. In the simulation, the boundary conditions are divided into two parts. The first part concerns the negative pressure within the cavities. This is achieved by applying negative pressure to all the inner shells of each cavity. The second part pertains to geometric constraints. We fixed the base of the device completely and then attached one side of the air chamber to the inner wall of the base. In the settings, we only used the 'Linear Elastic Material' since the device operates in the linear elastic range of Sylgard 184 ($< 15\%$). In this case, assuming linearity decreases the calculation time but does not affect the results. Based on the aforementioned settings, the COMSOL would automatically choose 'Linear tetrahedral elements' (Tet1) as the element type and the mesh size we chose is 'Normal'. (The total number of elements is 59639) Also, the 'Include geometric nonlinearity' is not chosen in the study setting since we didn't introduce hyperelastic model to this simulation.

E. Quantification of Strain Fields in Stretched Substrates

Strain quantification experiments were performed to determine the region of uniform strain in the stretched substrates and calibrate the pneumatic loading system. Specifically, fiduciary markers on the PDMS membranes were tracked using a video

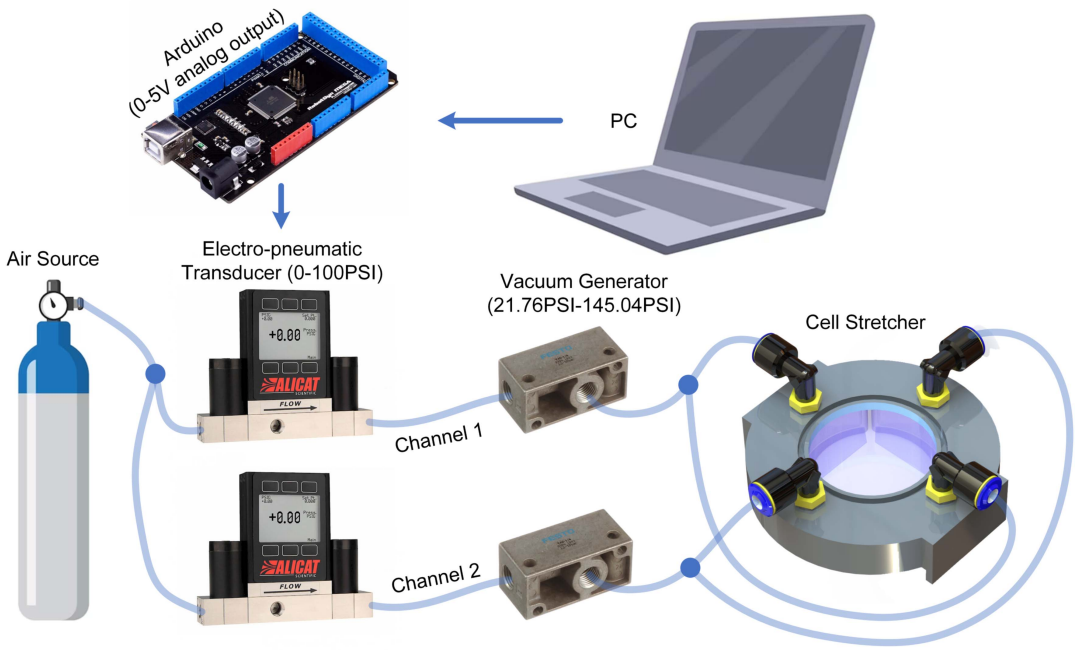

Fig. 3. Control system of biaxial cell-stretcher.

camera, under different stretch amplitudes and frequencies in both uniaxial and biaxial directions. From the acquired images, marker displacements were quantified using MATLAB (R2021a) between the reference and deformed configurations using particle tracking. A strain interpolation algorithm was implemented to quantify the in-plane Green-Lagrange strains from the marker displacements. [32].

F. Substrate Ligand Coating and Cell Culture

The PDMS membrane based stretching device was sterilized and the substrates were cleaned by ultrasonication using 70% ethanol followed by distilled water for 20 minutes each. The entire surface of the PDMS substrates were then coated with 3 ml of 80 $\mu g/mL$ collagen solution (Type I Collagen Solution, 4 mg/ml (Rat Tail)) at 37 °C for 1 h to facilitate cell attachment. Following which, the excess solution was then aspirated and the substrates were washed with PBS prior to seeding the cells. GFP expressing NIH-3T3 fibroblast cells were cultured on the coated PDMS substrates using Dulbecco's Modified Eagle Medium (DMEM) supplemented with 10% (v/v) fetal bovine serum (FBS) and 1% (v/v) penicillin/streptomycin in a sterile incubator with a humidified atmosphere containing 5% CO_2 at 37 °C. A cell seeding density of 1.25×10^4 $cells/cm^2$ was used for the stretching experiments. Cells were incubated overnight on the stretching device to allow attachment to the substrate prior to the stretching experiments.

G. Live-Cell Imaging Under Stretch

The pneumatically controlled stretching device with cells cultured on the PDMS membrane was mounted on a Leica DMI6000b epifluorescence microscope for real-time live imaging of cells under stretch. The microscope was housed inside a caged incubator (Pecon) equipped with temperature and CO_2 controllers, that helped maintain humidified atmosphere at 5% CO_2 and 37 °C required for prolonged cell viability. Cells were imaged with a 20x objective using bright-field and fluorescence microscopy to quantify changes in cell morphology under stretch. The obtained phase contrast images were then binarized and fundamental post-processing steps were implemented in ImageJ (NIH) to reduce background interference.We used a technique adapted from an earlier published work [32] to measure the cell orientations. Specifically, the cell images were binarized, following which a fast Fourier transformation (FFT) was calculated for the image. Next, we calculated the power spectrum of this matrix and obtained the spatial frequencies and orientations in Fourier space. A wedge-shaped orientation filter [33] was used to quantify the cellular orientation distributions in MATLAB. Cell stretching experiments were performed at 1 Hz for 3 hours for all sinusoidal strain combinations. Live-cell images were captured at 15-minute intervals. The loading briefly paused for a few seconds during capturing images, ensuring that each image taken was in a state without loading. At the beginning and end of each stretching process, we evaluated cell orientation, by capturing five images for each group from different regions of interest (ROI) within the central region of the membrane having uniform strain distributions. For each group under cyclic stretch, the total population of cells analyzed was greater than 150, and approximately 100 cells in each group for the static stretch experiments.

III. Results

A. System Characterization of Biaxial Cell Stretcher

The in-plane membrane strains were quantified by tracking fiducial markers on the PDMS using a particle tracking

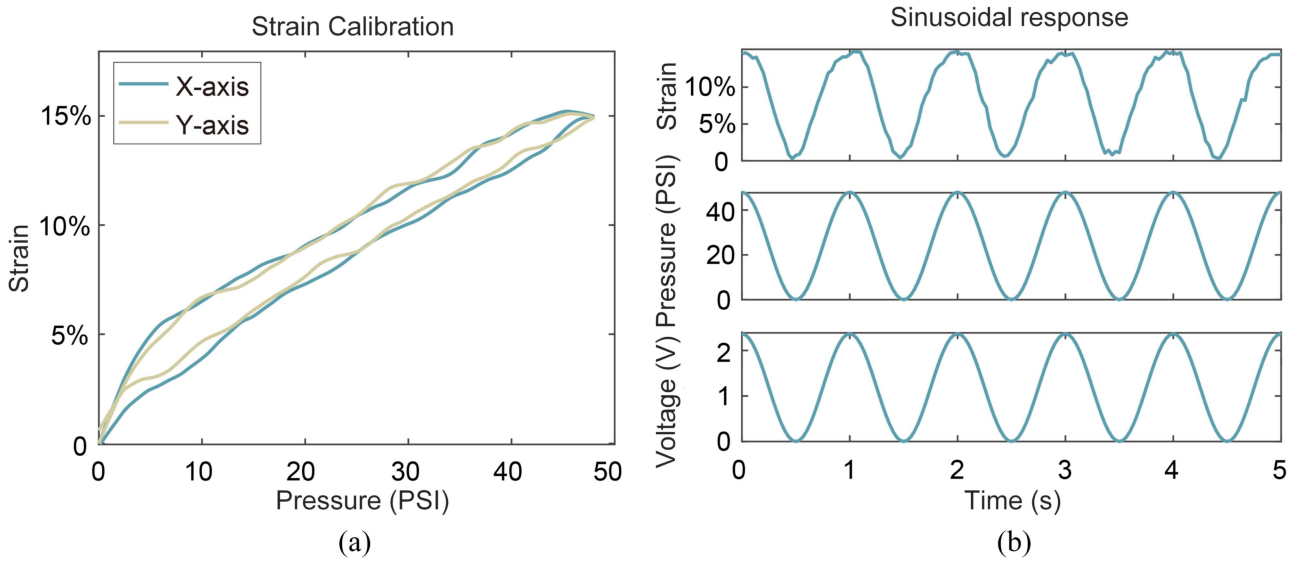

Fig. 4. System characterization of cell stretcher. (a) X-axis and Y-axis strain under continuous varying pressure. (b) uniaxial strain under sinusoidal loading.

algorithm. To characterize the strain-pressure relationship, we first applied a continuously varying pressure in the x and y directions separately as shown in Fig. 4(a) and Fig. S2. The result shows the change in strain is relatively linear, especially in the latter half when pressure decreases linearly. The strain in both directions reaches a maximum of 15% strain at $48PSI$. The nearly identical pressure-strain relationship in the x and y directions reflects the uniformity of the stretcher. As shown in Fig. 4(b), we validated the stretcher actuation under sinusoidal loading (1 Hz). The strain of the stretcher closely follows the sinusoidal pressure input. Also, we tested the actuation under triangle loading (1 Hz). However, the time required to fill and evacuate the pneumatic chambers creates a high-pass filter that smoothes the sharp peak of the triangle waveform near its maximum deformation. (Fig. S3) Therefore, in the following experiment, we chose sinusoidal loading as our input for cell experiments.

Our assessment of the cell stretcher's performance in response to varying frequencies involved two sets of tests (Fig. S4): one with uniaxial stretching and the other with equibiaxial stretching. In trials at frequencies of 1 Hz and lower, we observed no notable influence on the stretch attributes. However, a slight reduction in strain was noted at 2 Hz under higher input air pressures. It is important to note, though, that the operational range could still fulfill our requirements at this frequency. When the frequency was elevated to 5 Hz, a limitation became apparent. The stretching, both uniaxial and equibiaxial, failed to surpass a 7% strain, a constraint captured in Fig. S4. We assume this limitation is attributed to the viscoelasticity of the material we selected for our design. Nevertheless, the 2 Hz frequency threshold of the device satisfies the requirements for a wide range of biologically-relevant conditions.

Also, we have conducted supplementary experiments to assess the performance of our cell stretcher under continuous operation (Fig. S5). Here, the cell stretcher was exposed to a maximum equibiaxial stretching of 10% strain, facilitated by a 1 Hz sinusoidal input. We then evaluated the strain peaks along both the x-axis and y-axis at intervals of 0 hours, 4 hours, 8 hours, 12 hours, 24 hours, and 48 hours. The device shows consistent performance with no pronounced changes in the strain peaks over the 48-hour period. This underscores that prolonged maximum amplitude stretching does not compromise the mechanical integrity or performance of our cell stretcher.

Next, we validated the functionalities of the stretcher under sinusoidal loading. We compared three cases: uniaxial, equibiaxial and non-equibiaxial loading by experimentally quantifying the in-plane strains in each case. In the uniaxial case, we provide one channel of sinusoidal loading to only stretch the x-axis. The maximum strain amplitudes are calibrated to 5%, 10% and 15% with $16PSI$, $32PSI$ and $48PSI$, respectively. From Fig. 5(a), we observe that the device has a stable and repeatable sinusoidal response to the loading input, but the uniaxial stretching in x-axis can cause a heterophase strain change (20% of the x-axis strain) in y-axis. This Poisson effect has been reported in other uniaxial stretcher work [30], [32]. However, for our biaxial stretcher, the actuation in the other direction is able to compensate for the Poisson effect. FE simulations in Fig. 5(b) show that the membrane exhibits uniform strain with average E11 (x-axis strain) of 5.1%, 10.2%, 15.3%, respectively and average E22 (y-axis strain) -1.2%, -2.5%, -3.8%, respectively, which corresponds well with the experimental measurements. In the equibiaxial case, we provide two channels of homophase sinusoidal loading. As shown in Fig. 5(c), when applying $30PSI - 29PSI$ in both channels, the stretcher can obtain exactly 5% strain in both directions. Similarly, when applying $49PSI - 48PSI$ and $65PSI - 64PSI$, equibiaxial strains of 7.5% and 10% could be obtained. The slight difference in the calibrated pressures may be caused by small variations in the pneumatic controls for the two independent channels. Example sources of these errors could include variations in the length of the tube used to connect the

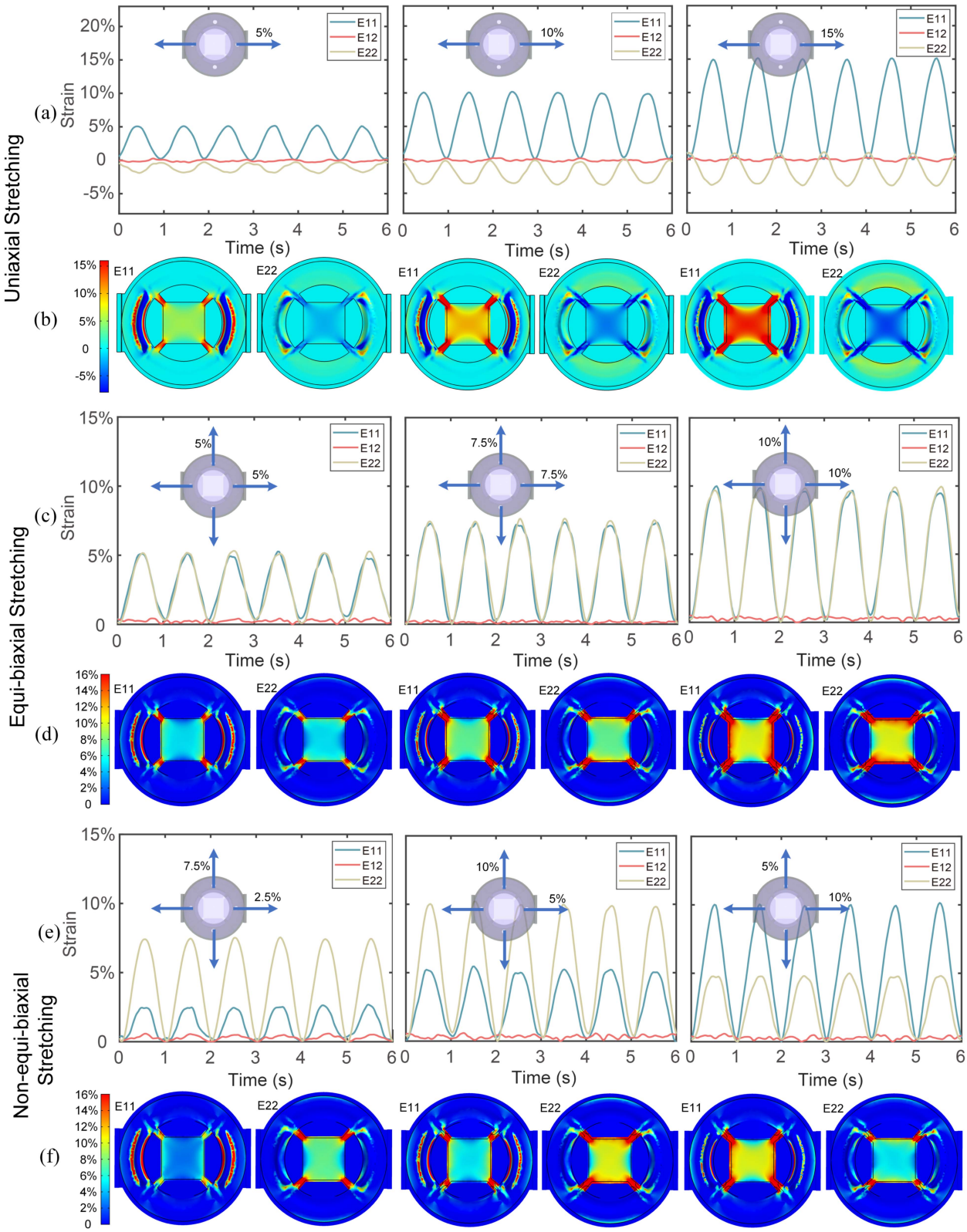

Fig. 5. Demonstration of the functionalities of biaxial cell stretcher. (a)–(b) Experimental results and simulation results of uniaxial stretching of 5%, 10%, and 15% under 1 Hz sinusoidal loading. The relevant pressure input is $16PSI$, $32PSI$, and $48PSI$. (c)–(d) Experimental results and simulation results of equibiaxial stretching of 5%, 7.5%, and 10% under 1 Hz sinusoidal loading. The relevant pressure input is $30PSI - 29PSI$, $49PSI - 48PSI$ and $65PSI - 64PSI$. (e)–(f) Experimental results and simulation results of non-equibiaxial stretching of 2.5%–7.5%, 5%–10%, and 10%–5% under 1 Hz sinusoidal loading. The relevant pressure input is $24PSI - 48PSI$, $37PSI - 53PSI$, and $55PSI - 35PSI$.

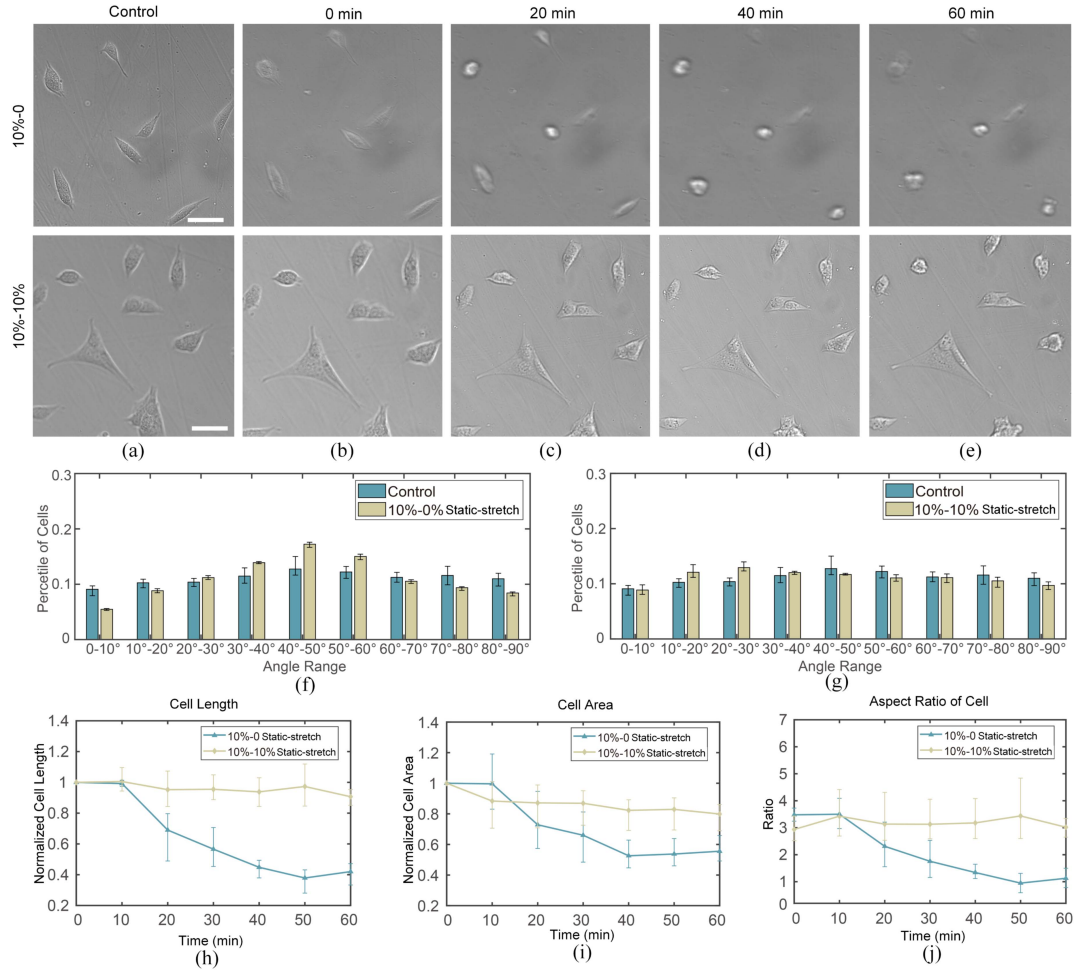

Fig. 6. Cells subjected to static stretch under uniaxial and biaxial loading shown with bright field microscopy images (unprocessed cell images). (a)–(e) Live-cell images of unstretched membrane (Control) and stretched membrane every 20 min. (f) Cell orientation changes after applying 1 h static stretch. (g)–(i) depicts the changes in single cell morphology, where (g) shows the normalized length change of cells and (h) shows the area change of cells under two different stretching conditions. (i) displays the aspect ratio (ratio of the major to minor axes for individual cells, with the assumption that cells exhibit an elliptical shape). The white scale bar in (a)–(e) refers to $50\ \mu\mathrm{m}$.

stretcher to the vacuum source or the calibration error of the pressure controller. The unique capability of this stretcher to generate strains in two directions independently is demonstrated using 3 example cases of strains in the x-y directions: 2.5%–7.5%, 5%–10%, and 10%–5%. For each example, the corresponding input pressure is $24PSI - 48PSI$, $37PSI - 53PSI$, and $55PSI - 35PSI$, respectively. Fig. 5(d) and (f) depicts the FE simulation results that are under the same pressure conditions of biaxial stretching. The results agree with their relevant experimental measurements within 5% error in both directions. Based on the localized zoom-ins for simulation illustrated in Fig. S6-8, we can observe that in the central area of biaxial stretching, over 70% of the region enclosed by stickers experiences strain variations less than $\pm 1\%$, which can be regarded as the working area. Although the working area slightly decreases as the strain increases, the reduction is not substantial. In contrast, for uniaxial stretching, the uniform central area is relatively smaller and the trend of decrease with strain variation is quite apparent. Moreover, given that our apparatus has the capability to exert distinct forces in two directions, it allows the realization of a unique non-equibiaxial scenario. In this context, while one direction undergoes a specific strain, the exerted pressure in the perpendicular direction can fully counteract the Poisson effect, resulting in a 0% strain in that direction. This is exemplified in cases of 5%–0% ($28PSI - 12PSI$) and 10%–0% ($48PSI - 20PSI$) as presented in Fig. S9, accompanied by the corresponding FE simulation results.

B. Live-Cell Images on Static-Stretched Membrane

A significant advantage of the proposed cell stretching device is the ability to capture high-quality live-cell images through the stretchable PDMS membrane.To capture stable images, we stretched the membrane uniaxially and biaxially to 10% static strain and recorded live-cell images every 10 min (Fig. 6). All images were captured in real-time directly from the microscope without any post-processing. Compared to the control (no strain), the 0 min (10% strain) images indicate that the adherent 3T3 cells are sensitive to the applied strain on the underlying membrane which affects their relative position and morphology. Application of static stretch results in an increase in the cellular traction forces [34], causing cells to realign under loading.

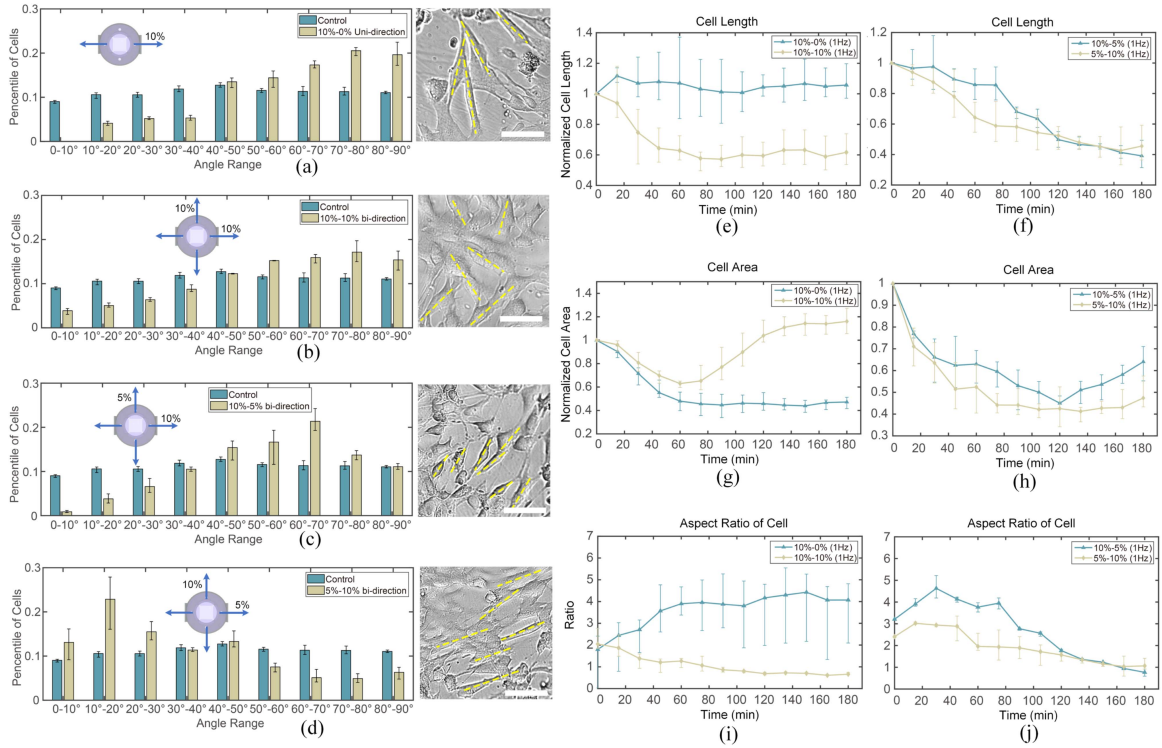

Fig. 7. Changes in cell orientation and morphology after 3 hours of cyclic stretching. (a) Cell orientation change after 3 hours 10%–0 uniaxial stretching. (b) Cell orientation change after 3 hours 10%–10% equibiaxial stretching. (c) Cell orientation change after 3 hours 10%–5% non-equibiaxial stretching. (d) Cell orientation change after 3 hours 5%–10% non-equibiaxial stretching. The angle under consideration represents the inclination relative to the x-axis (horizontal). 0° denotes alignment parallel to the x-axis, whereas 90° indicates orientation perpendicular to the x-axis. (e)–(j) depicts the morphology change of single cells, where (e)–(f) shows the normalized length change of cells and (g)–(h) shows the normalized area change of cells under four stretching conditions. (i)–(j) displays the aspect ratio (ratio of the major to minor axes) for individual cells, with the assumption that cells exhibit an elliptical shape. In (a)–(d), we show the bright field microscopy images (unprocessed cell images) after 3 hours stretching and have used yellow dashed lines to indicate the orientation of the cells. The white scale bar in (a)–(d) refers to $40\ \mu\mathrm{m}$.

However, these responses are dependent on underlying substrate stiffness that dictates the strength and stability of these focal adhesions, which may influence the detachment of some of the cells during realignment under stretch. Further, the distribution of cellular orientation under static stretch is generally wider as compared to cyclic stretch [35], [36] and are highly attenuated on stiffer substrates often leading to random alignments [37]. We hypothesize that the changes in cellular orientation under static stretch are influenced by the stiffness of the PDMS substrate similar to an earlier study by Jungbauer et al. [37]. Under uniaxial static stretch, we observe a reduction in the cell spread area and length. We hypothesize this may be linked with the focal adhesion dynamics which causes cellular realignment under stretch. Detachment of the cells from the stretched membrane, can depend on the strength and stability of the focal adhesion complexes. For the biaxial case, we do not see a significant change in the cellular morphometrics, like cell area and aspect ratio, which may be linked with the direction-dependent changes in cellular contractility under stretch.

We performed a quantitative assessment of cellular orientation and morphology change of individual cells, as illustrated in Fig. 6. The application of 1-hour static uniaxial stretching resulted in not only partial cell detachment but also a gradual realignment of the initially uniformly distributed cells in the orthogonal direction, leading to a major angle of approximately 45 degrees. In contrast, the 1-hour static biaxial stretching demonstrated minimal influence on cell orientation. We employed single-cell tracking to quantify changes in cellular morphology. Initially, we monitored alterations in the length and area of 3 individual cells.(Fig. 6(g) and (h)) Subsequently, by assuming an elliptical cell shape, we calculated the ratio between the major and minor axes for more intuitive description shown in Fig. 6(i)). The raw data for Fig. 6(g)–(i) is shown in Fig. S10. Uniaxial stretching leads to a reduction in cell length and causes detached cells to adopt a more circular shape. In contrast, biaxial static stretching does not induce any significant morphological changes in cells. Notably, while a subset of cells becomes thinner, another subset appears to become more rounded.

C. Cellular Orientation and Morphology Change Under Cyclic Stretching With Different Strain Conditions

To verify the functionality of the device in cell experiments, we quantified cell alignment under four distinct stretching conditions: 10%–0% uniaxial stretching, 10%–10% equibiaxial stretching, 10%–5% and 5%–10% non-equibiaxial stretching. As demonstrated in Fig. 7(a), uniaxial stretching results in cellular realignment perpendicular to the stretch direction. Under equibiaxial stretching, we observe that the magnitude of cellular realignment is relatively less pronounced. While a

large fraction of the cell population are aligned within about 60–80 ° range, these percentiles are significantly lesser as compared under uniaxial stretch (Fig. 7(b)). Previous studies by Livne et al. [38] showed that for cyclic stretch with different biaxiality ratios the cellular alignment ranged between 50 to 70 degrees. Theoretical investigations by Xu et al. [34] have also shown similar trends when the strain amplitude is within 10%. These studies corroborate with the initial measurements reported in our study. Non-equibiaxial cell stretching is also capable of inducing notable alterations in cell orientation. For the 10%–5% scenario, the predominant cell angles span from 50 to 70 degrees, attributable to the higher strain experienced in the x-direction. In contrast, the 5%–10% situation exhibits primarilay cellular orientation angles between 10 and 30 degrees, resulting from the higher strain present in the y-direction.

Additionally, utilizing the live-cell images acquired during the experiment, we monitored the area and length alterations of 5 individual cells in each case. Here, we first transform the image series collected during the cell stretching into a video and then used the Direct Linear Transformation (DLT) digitizing tool implemented in Matlab. It can automatically track and analyze objects in video sequences (Developed by Ty Hedrick from UNC). [39] When selecting tracking cells, we chose five cells with initial orientations closely aligned with the y-axis. Within the DLTdv8a, the two vertices of the cells' longer edges were selected for tracking. If the auto-track is interrupted due to sudden shape change of cells between frames or insufficient image clarity, manual selection of the tracking points is employed. From this data, we obtained the variation in cell length over time. (Fig. 7) Subsequently, we monitor the alterations in the area of these cells by initially delineating the cellular contours and subsequently quantifying the pixel counts associated with respective shapes. (Fig. 7) To more effectively illustrate the morphology change of the cells from the data, we posited that the cell's overall shape is elliptical.

Then, we derived the ratio of the major and minor axes by the data of the cell's length and area. Fig. 7(e) and (f) demonstrates that uniaxial stretching leads to an increased elongation of the cell and a decrease in overall cell area (Fig. 7(g)), while biaxial stretching results in a more rounded cellular morphology (Fig. 7(g)). We also observe that the changes in cell length and area under the application of non-equibiaxial stretch follow similar trends irrespective of the direction of applied stretches (Fig. 7(f) and (h)). Finally, the changes in cellular aspect ratio corroborate with the changes in cell length and area with cells becoming more elliptical under uniaxial stretch as compared to equibiaxial stretch (Fig. 7(i)). The aspect ratio changes under anisotropic stretch show analogous responses for both 10%–5% and 5%–10% stretch.

IV. Discussion

In this article, we describe a custom mechanobiological platform that enables measuring cellular responses to non-equibiaxial strains over a range of frequencies and strain magnitudes. This first manifestation of the platform described in this manuscript has been designed with a large cell growth area ($2\,\mathrm{cm} \times 2\,\mathrm{cm}$) for cell attachment and visualization. However, our design can be scaled to smaller or larger dimensions based on the needs of the research. Compared with microscale cell growth area [30], [40], larger culture areas provide a more homogenous strain field that could provide more reliable and robust results. Furthermore, our scalable cell culture area could be advantageous for studies necessitating a high cell count or the collection of multiple samples from a single culture.

While this work was demonstrated with 2D cell cultures, it is widely accepted that 3D cell cultures more closely replicate the in vivo environment. [41], [42] To theoretically evaluate the ability to facilitate 3D cell culture, we have used finite element simulations to determine the impact of an appropriate thickness of collagen ($30\ \mu\mathrm{m}$) on membrane stretching. The presence of a cell-laden collagen gel with a Young's modulus of $15\,\mathrm{kPa}$ [43] does not significantly affect the membrane's stretching performance because its stiffness is significantly lower than that of the membrane. The results revealed that, under the same conditions, a membrane with 30 μm collagen stretched to a 10% strain while a membrane without collagen reached a 10.4% strain. Consequently, the presence of collagen only introduces discrepancy of around 4%, which can be corrected in the calibration process.

The last several decades of mechanobiology research have emphasized the breadth of parameters that affect cell growth, including the modulus, porosity, and viscoelasticity of the extracellular environment in addition to chemical stimuli. Increasing evidence shows that these factors can be interdependent, necessitating the performance of combinatorial measurements to elucidate their effects. [44], [45], [46], [47] These combinatorial measurements require parallel experiments on many conditions simultaneously, which could be enabled by the low cost of our system.

The material cost of each stretcher priced at approximately $10 (including the 3D print resin and PDMS). The cost of the pneumatic controls includes the tubes, transducers, vacuum generators, and Arduino. The total cost could be around $3000. However, since the cost of each cell stretcher is only $10, when a system hosts 10 parallel-operating cell stretchers, the average cost for each is approximately $310 for the initial purchase. The pneumatic controls can be reused, so the initial purchase could be amortized over all experiments. Following the completion of the 3D-printed mold, the device can be affordably mass-produced. As a single control system can simultaneously manage more than 10 stretchers, its control system cost is relatively low compared to motor-driven cell stretchers, each of which requires an individual motor for operation. Concurrently, upon the conclusion of cell culturing, reusability can be attained through membrane replacement. Provided that the membrane's thickness remains consistent and uniform, the error resulting from membrane substitution can be maintained below 3%. Moreover, as all chambers are generated from an identical mold, the variability between stretchers is less than 5%, primarily attributable to manual assembly in laboratory settings. It is anticipated that the error will decrease further with the implementation of industrial-scale mass production.

The main cost of the system is the pneumatic controls. Our system exhibits an average pumping speed of $30\,\mathrm{L/min}$, while the individual chamber volume is approximately $1\,\mathrm{cm}^3$. Consequently, the time delay between operating 10 stretchers concurrently versus a single stretcher is less than 0.04 seconds, which is much smaller than the rate at which we actuate the devices (1 Hz). This indicates that a single pneumatic control system can efficiently actuate over 10 stretchers simultaneously, which allows for higher-throughput studies.

V. Conclusion

In this work, we present a novel cell stretching system that enables independent control of orthogonal in-plane strains on a deformable membrane, through which live-cell imaging is possible. Uniaxial and biaxial cell stretching devices are useful to quantify cellular response to complex mechanical stimulation, which could give insights into tissue development or disease progression. Our strain calibration experiments show that our custom stretching device can provide controllable multiaxial mechanical stimuli. Due to the in-plane deformation of the cell culture membrane, real-time imaging was used to track the cell size and orientation as a function of static and cyclic strains. Significant differences were observed in the cell aspect ratio and alignment when using the non-equibiaxial strains enabled by our device compared to the uniaxial and biaxial strains that are commonly used. We believe our device will be useful for conducting a range of mechanobiological studies, providing useful insights into cell behavior in the context of disease diagnosis and development.

References

[1] V. Vogel and M. Sheetz, "Local force and geometry sensing regulate cell functions," *Nature Rev. Mol. Cell Biol.*, vol. 7, no. 4, pp. 265–275, 2006.

[2] X.-M. Gao et al., "Post-infarct cardiac rupture: Recent insights on pathogenesis and therapeutic interventions," *Pharmacol. Therapeutics*, vol. 134, no. 2, pp. 156–179, 2012.

[3] O. Gültekin, G. Sommer, and G. A. Holzapfel, "An orthotropic viscoelastic model for the passive myocardium: Continuum basis and numerical treatment," *Comput. Methods Biomech. Biomed. Eng.*, vol. 19, no. 15, pp. 1647–1664, 2016.

[4] W. M. Torres et al., "Regional and temporal changes in left ventricular strain and stiffness in a porcine model of myocardial infarction," *Amer. J. Physiol.-Heart Circulatory Physiol.*, vol. 315, no. 4, pp. H958–H967, 2018.

[5] A. D. Rouillard and J. W. Holmes, "Mechanical regulation of fibroblast migration and collagen remodelling in healing myocardial infarcts," *J. Physiol.*, vol. 590, no. 18, pp. 4585–4602, 2012.

[6] C. J. Philp et al., "Extracellular matrix cross-linking enhances fibroblast growth and protects against matrix proteolysis in lung fibrosis," *Amer. J. Respir. Cell Mol. Biol.*, vol. 58, no. 5, pp. 594–603, 2018.

[7] F. J. Martinez et al., "Idiopathic pulmonary fibrosis," *Nature Rev. Dis. Primers*, vol. 3, no. 1, pp. 1–19, 2017.

[8] E. Yamamoto et al., "Development of residual strains in human vertebral trabecular bone after prolonged static and cyclic loading at low load levels," *J. Biomech.*, vol. 39, no. 10, pp. 1812–1818, 2006.

[9] D. D. Chan et al., "In vivo articular cartilage deformation: Noninvasive quantification of intratissue strain during joint contact in the human knee," *Sci. Rep.*, vol. 6, no. 1, pp. 1–14, 2016.

[10] K. Naruse, T. Yamada, and M. Sokabe, "Involvement of sa channels in orienting response of cultured endothelial cells to cyclic stretch," *Amer. J. Physiol.-Heart Circulatory Physiol.*, vol. 274, no. 5, pp. H1532–H1538, 1998.

[11] Y. Shao et al., "Uniaxial cell stretching device for live-cell imaging of mechanosensitive cellular functions," *Rev. Sci. Instruments*, vol. 84, no. 11, 2013, Art. no. 114304.

[12] S. Leung et al., "A novel in vitro and in silico system for analyzing complex mechanobiological behavior of chondrocytes in three-dimensional hydrogel constructs," *J. Biomechanical Eng.*, vol. 143, no. 8, 2021, Art. no. 084503.

[13] L. A. McMahon et al., "Regulatory effects of mechanical strain on the chondrogenic differentiation of MSCs in a collagen-GAG scaffold: Experimental and computational analysis," *Ann. Biomed. Eng.*, vol. 36, pp. 185–194, 2008.

[14] B. J. Pfister et al., "An in vitro uniaxial stretch model for axonal injury," *Ann. Biomed. Eng.*, vol. 31, pp. 589–598, 2003.

[15] A. Poulin et al., "An ultra-fast mechanically active cell culture substrate," *Sci. Rep.*, vol. 8, no. 1, 2018, Art. no. 9895.

[16] Y. Iwadate and S. Yumura, "Cyclic stretch of the substratum using a shape-memory alloy induces directional migration in dictyostelium cells," *Biotechniques*, vol. 47, no. 3, pp. 757–767, 2009.

[17] D. Wang et al., "A stretching device for imaging real-time molecular dynamics of live cells adhering to elastic membranes on inverted microscopes during the entire process of the stretch," *Integrative Biol.*, vol. 2, no. 5/6, pp. 288–293, 2010.

[18] D. Huh et al., "Reconstituting organ-level lung functions on a chip," *Science*, vol. 328, no. 5986, pp. 1662–1668, 2010.

[19] H. Kamble et al., "Pneumatically actuated cell-stretching array platform for engineering cell patterns in vitro," *Lab a Chip*, vol. 18, no. 5, pp. 765–774, 2018.

[20] S. Correia Carreira et al., "Flexert: A soft, actuatable multiwell plate insert for cell culture under stretch," *ACS Biomaterials Sci. Eng.*, vol. 7, no. 6, pp. 2225–2245, 2021.

[21] Y. Huang and N.-T. Nguyen, "A polymeric cell stretching device for real-time imaging with optical microscopy," *Biomed. Microdevices*, vol. 15, pp. 1043–1054, 2013.

[22] J. Kreutzer et al., "Pneumatic unidirectional cell stretching device for mechanobiological studies of cardiomyocytes," *Biomech. Model. Mechanobiol.*, vol. 19, pp. 291–303, 2020.

[23] A. A. Lee et al., "Differential responses of adult cardiac fibroblasts to in vitro biaxial strain patterns," *J. Mol. Cellular Cardiol.*, vol. 31, no. 10, pp. 1833–1843, 1999.

[24] F. Bieler et al., "Biaxial cell stimulation: A mechanical validation," *J. Biomech.*, vol. 42, no. 11, pp. 1692–1696, 2009.

[25] C. P. Ursekar et al., "Design and construction of an equibiaxial cell stretching system that is improved for biochemical analysis," *PLoS One*, vol. 9, no. 3, 2014, Art. no. e90665.

[26] H. Peussa et al., "Pneumatic equiaxial compression device for mechanical manipulation of epithelial cell packing and physiology," *Plos One*, vol. 17, no. 6, 2022, Art. no. e0268570.

[27] J.-U. Voigt and M. Cvijic, "2-and 3-dimensional myocardial strain in cardiac health and disease," *JACC: Cardiovasc. Imag.*, vol. 12, no. 9, pp. 1849–1863, 2019.

[28] E. Wong et al., "Design of a mechanobioreactor to apply anisotropic, biaxial strain to large thin biomaterials for tissue engineered heart valve applications," *Ann. Biomed. Eng.*, vol. 50, no. 9, pp. 1073–1089, 2022.

[29] J.-J. Hu, J. D. Humphrey, and A. T. Yeh, "Characterization of engineered tissue development under biaxial stretch using nonlinear optical microscopy," *Tissue Eng. Part A*, vol. 15, no. 7, pp. 1553–1564, 2009.

[30] D. Tremblay et al., "A microscale anisotropic biaxial cell stretching device for applications in mechanobiology," *Biotechnol. Lett.*, vol. 36, pp. 657–665, 2014.

[31] C. Hart et al., "Biocompatibility of blank, post-processed and coated 3D printed resin structures with electrogenic cells," *Biosensors*, vol. 10, no. 11, 2020, Art. no. 152.

[32] A. Chatterjee, P. Kondaiah, and N. Gundiah, "Stress fiber growth and remodeling determines cellular morphomechanics under uniaxial cyclic stretch," *Biomech. Model. Mechanobiol.*, vol. 21, no. 2, pp. 553–567, 2022.

[33] A. H. Kulkarni et al., "Tgf-β induces changes in breast cancer cell deformability," *Phys. Biol.*, vol. 15, no. 6, 2018, Art. no. 065005.

[34] G.-K. Xu, X.-Q. Feng, and H. Gao, "Orientations of cells on compliant substrates under biaxial stretches: A theoretical study," *Biophysical J.*, vol. 114, no. 3, pp. 701–710, 2018.

[35] C. Liu et al., "Effect of static pre-stretch induced surface anisotropy on orientation of mesenchymal stem cells," *Cellular Mol. Bioeng.*, vol. 7, pp. 106–121, 2014.

[36] A. M. Collinsworth et al., "Orientation and length of mammalian skeletal myocytes in response to a unidirectional stretch," *Cell tissue Res.*, vol. 302, pp. 243–251, 2000.
[37] S. Jungbauer et al., "Two characteristic regimes in frequency-dependent dynamic reorientation of fibroblasts on cyclically stretched substrates," *Biophysical J.*, vol. 95, no. 7, pp. 3470–3478, 2008.
[38] A. Livne, E. Bouchbinder, and B. Geiger, "Cell reorientation under cyclic stretching," *Biophysical J.*, vol. 106, no. 2, 2014, Art. no. 42a.
[39] T. L. Hedrick, "Software techniques for two-and three-dimensional kinematic measurements of biological and biomimetic systems," *Bioinspiration Biomimetics*, vol. 3, no. 3, 2008, Art. no. 034001.
[40] Q. Wang et al., "Microscale cell stretcher to generate spatially uniform equi-biaxial strain using an elastomeric membrane with a contoured thickness profile," *Sensors Actuators B: Chem.*, vol. 273, pp. 1600–1609, 2018.
[41] K. Chen et al., "Role of boundary conditions in determining cell alignment in response to stretch," *Proc. Nat. Acad. Sci.*, vol. 115, no. 5, pp. 986–991, 2018.
[42] C. Jensen and Y. Teng, "Is it time to start transitioning from 2D to 3D cell culture ?," *Front. Mol. Biosciences*, vol. 7, 2020, Art. no. 33.
[43] M. Lopez-Garcia, D. Beebe, and W. Crone, "Young's modulus of collagen at slow displacement rates," *Bio- Med. Mater. Eng.*, vol. 20, no. 6, pp. 361–369, 2010.
[44] J. Seo et al., "Interconnectable dynamic compression bioreactors for combinatorial screening of cell mechanobiology in three dimensions," *ACS Appl. Mater. Interfaces*, vol. 10, no. 16, pp. 13293–13303, 2018.
[45] H. Liu et al., "Combinatorial screen of dynamic mechanical stimuli for predictive control of MSC mechano-responsiveness," *Sci. Adv.*, vol. 7, no. 19, 2021, Art. no. eabe7204.
[46] A. M. Throm Quinlan et al., "Combining dynamic stretch and tunable stiffness to probe cell mechanobiology in vitro," *PLoS One*, vol. 6, no. 8, 2011, Art. no. e23272.
[47] Y. Cui et al., "Cyclic stretching of soft substrates induces spreading and growth," *Nature Commun.*, vol. 6, no. 1, 2015, Art. no. 6333.